

**Title:** Applicability of hypoplasticity to reconstituted peat from drained triaxial tests

**Authors**

S. Muraro\*

D. Mašín\*\*

C. Jommi\*, \*\*\*

**Affiliation**

\* Department of Geoscience and Engineering, Delft University of Technology, Stevinweg 1, 2628 CN, Delft, The Netherlands

\*\* Institute of Hydrogeology, Engineering Geology and Applied Geophysics, Charles University, Albertov 6, 128 43 Prague 2, Prague, Czech Republic

\*\*\* Department of Civil and Environmental Engineering, Politecnico di Milano, piazza Leonardo da Vinci 32, 20133 Milano, Italy

**Keywords**

Laboratory tests, drained triaxial tests, peat, constitutive modelling, hypoplasticity

**Correspondence to**

Stefano Muraro, Department of Geoscience and Engineering

Delft University of Technology, Stevinweg 1 / PO-box 5048, 2628 CN Delft, The Netherlands

Tel. +31 15 27 83327; e-mail: S.Muraro@tudelft.nl

## **ABSTRACT**

Proper understanding of the deviatoric behaviour of peats represents a challenge in soil mechanics. Exceptional high compressibility together with extremely high friction angles distinguish peats from classical organic soils. Considerable amount of triaxial tests data on peats can be found in the literature, mostly coming from standard undrained triaxial compression tests. However, only a minor part was intended to describe their pre-failure behaviour. Also, limiting the investigation to the undrained response, reduces the information on those ingredients of constitutive models, which are necessary to describe the deformational behaviour. This contribution aims to provide better insight into the pre-failure deformational behaviour of peats, by analysing in detail the results of non-standard drained tests at various stress paths, and undrained tests performed on reconstituted peat samples. Based on the experimental findings, an existing hypoplastic model, originally developed for fine-grained soils, has been adapted to capture the behaviour of peats. The model is directly calibrated on selected experimental results and validated on a variety of different stress paths tests. The results reveal the merits of hypoplasticity in modelling the non-linearity of the pre-failure behaviour and the directional response of peats, which both are of great importance when assessing the serviceability limit states of geotechnical structures founded on peats.

## INTRODUCTION

Extensive experimental research has been carried out so far on peats, mainly using undrained triaxial compression tests. These tests have been focused mostly on the shear strength, and elucidated the frictional nature of the peat fabric with small apparent intercept cohesion and high friction angles in the range of  $50^{\circ}$ - $70^{\circ}$  (Adams [1]; Landva and La Rochelle [2]; Yamaguchi et al. [3]; Farrell and Hebib [4]; Edil and Wang [5]; Cola and Cortellazzo [6]; Cheng et al. [7]). The presence of multiple fibrous networks not entirely decomposed within the peat fabric is recognised to provide additional reinforcement to the material, hence justifying the high shear strength parameters (Landva and La Rochelle [2]).

Despite the considerable amount of laboratory investigation on the shear behaviour of peats, only a minor part was intended to describe the mechanical behaviour before ultimate state conditions. However, the design and the assessment criteria in many geotechnical applications where peats are encountered, are ruled by serviceability limit states rather than ultimate limit states.

These considerations call for an adequate geotechnical description of the pre-failure response of these materials. The volumetric behaviour of peat, with particular attention to creep, has been widely investigated both from the experimental and the constitutive viewpoints (Berry and Poskitt [8]; Berry and Vickers [9]; Landva and La Rochelle [2]; Lefebvre et al. [10]; Tsushima [11]; Fox et al. [12]; Edil et al. [13]; Fox and Edil [14]; Den Haan and Edil [15]; Mesri et al. [16]; Den Haan and Kruse [17]; Mesri and Ajlouni [18]; Madaschi and Gajo [19]; Acharya et al. [20]; Fox et al. [12]; Den Haan [21] and Madaschi and Gajo [22]). However, only few contributions focus on the modelling of the deviatoric behaviour of peats. The first attempt is due to Yamaguchi et al. [3], who developed an elastic-plastic model based on the Modified Cam clay (Roscoe and Burland [23]), which was coupled with an experimentally based stress-dilatancy law. The model was capable to capture the ultimate state detected in undrained compression triaxial tests, but with a significant overestimation of the stiffness in the deviatoric stress-strain response. Recent attempts include the

application of the Soft Soil Creep model, Den Haan and Feddema [24], and its anisotropic version, Den Haan [25], based on the original works by Leoni et al. [26], Vermeer and Neher [27] and Wheeler et al. [28]. A kinematic bubble model was proposed by Boumezerane [29], based on Al-Tabbaa and Wood [30] and Sivasithamparam [31]. More recently, Yang et al. [32] adopted the elastic-plastic model by Li and Dafalias [33] to reproduce undrained triaxial compression tests on reconstituted peat samples, while Boumezerane et al. [34] suggested the use of an hyperplastic model.

The vast majority of the previous models have been calibrated and tested based on experimental results coming from undrained triaxial compression tests. However, undrained tests do not allow to determine directly some of the main constitutive ingredients, such as the yield locus and the stress-dilatancy relationship for the case of a general elastic-plastic framework.

To overcome this limitation, a series of non-standard drained triaxial tests have been carried out on reconstituted peat samples, especially focussing on the pre-failure deformational behaviour. Based on the experimental results, a simple model for reconstituted peat is developed starting from an existing hypoplastic approach originally proposed for clays (Mašín [35], [36]). This choice is based on the capability of hypoplasticity to predict a smooth transition between overconsolidated and normally consolidated states and to account for the non-linear pre-failure response, which appears to be of great relevance for the case of peats. The constitutive ingredients of the hypoplastic model have been explicitly derived from the results of drained tests with multiple loading-unloading stress paths. Particular attention has been given to the definition of asymptotic states, namely the boundary surface and the corresponding asymptotic strain rate directions. The modelling effort has a twofold scope: it allows elucidating the hypoplastic modelling ingredients for peats, and it provides a reference hypoplastic model, on which further relevant features, such as anisotropy and creep can be added.

## EXPERIMENTAL PROGRAMME

### Stresses and strain variables

All the experimental data have been elaborated herein by assuming axisymmetric test conditions. The complete description of the soil stress state is accomplished by adopting the common triaxial stress variables: mean effective stress  $p'$ , and deviatoric stress  $q$ . For the conjugate strain variables, volumetric strain,  $\varepsilon_p$ , and deviatoric strain,  $\varepsilon_q$ , are considered. Large displacements typically reached when testing peat call for the adoption of the natural strains in the present work (Ludwik [37]; Hencky [38]). Natural strains imply the validity of the additive principle in eq. (1) at small as well as at large strains. In the absence of direct measurement of the radial displacements, the deviatoric strain has been computed from the volume change and the axial displacement measurements (i.e.  $\varepsilon_p$  and  $\varepsilon_a$ ):

$$\varepsilon_p = \varepsilon_a + 2\varepsilon_r = \ln\left(\frac{V_0}{V}\right) \quad (1)$$

$$\varepsilon_q = \varepsilon_a - \frac{\varepsilon_p}{3} = \ln\left(\frac{H_0}{H}\right) - \frac{1}{3}\ln\left(\frac{V_0}{V}\right) \quad (2)$$

where  $V_0$  and  $H_0$  are the initial volume and the initial height of the sample, while  $V$  and  $H$  are the current values. The cross sectional area of the specimen has been corrected by assuming a right equivalent cylinder (Head and Epps [39]). Comparison between the calculated diameters and the ones measured at the end of each test supported this choice.

### Tested material and experimental methodology

The experimental study was conducted on peat collected from the Leendert de Boerspolder site in the Netherlands. The material was collected from a surficial peat deposit 1.5 m below the ground surface. To reduce bio-degradation, the material was stored in a climate controlled room at  $10 \pm 1^\circ\text{C}$

and 90% relative humidity. Reconstituted peat samples were prepared for all the tests according to the following procedure. The material was mixed with demineralised water to slurry with water content of 855%, which corresponds to 1.4 times the limit liquid. The material was then consolidated in a floating consolidometer under a total vertical stress of 9.5 kPa for 48 hours. The reconstituted sample was then extracted and mounted in the triaxial apparatus. All the tests were performed under strict controlled air temperature  $14 \pm 1^\circ\text{C}$  and relative humidity 80%. To prevent loss of organic matter, the oven-drying procedures for the classification of the tested material were performed at a temperature of  $60^\circ\text{C}$  (Head [40]). The specific gravity  $G_s$ , of the soil was measured with a helium pycnometer in accordance with ASTM D5550–14 (ASTM [41]). The organic content OC, was assessed by ignition in a furnace at  $500^\circ\text{C}$  (ASTM [42]; Den Haan and Kruse [17]). Table 1 reports the index properties of the tested samples. The average fibre content was 0.14 (ASTM [43]).

The nominal dimensions of the tested specimens were 50 mm in diameter and 100 mm in height. All the tests were carried out using a load frame type GDS triaxial system, with back pressure and cell pressure volume controllers, and a submersible 1 kN load cell. Thin membranes 0.25 mm thick were used. To accelerate the consolidation process, lateral filter paper was placed around the samples. To prevent “short circuit” effects between the back pressure and the pore pressure transducers, 10 mm clearance were left between the lower edge of the lateral filter paper and the bottom of the samples (Head and Epps [39]). Each vertical drainage strip had free lower end to reduce the potential contribution offered by the lateral filter paper to the measured strength of the material.

**Table 1** Index properties and relevant stress variables of the tested specimens

Sample	Specific gravity	Initial void ratio	Organic content	Preconsolidation stress	Stress before shearing	Over-consolidation ratio	Drainage conditions
	G <sub>s</sub>	e <sub>0</sub>	OC	p' <sub>0</sub>	p' <sub>start shear</sub>	OCR	
	[-]	[-]	[-]	[kPa]	[kPa]	[-]	
1	1.52	9.8	0.91	74	18	4.1	Drained
2	1.49	9.8	0.91	32	14	2.3	Drained
3	1.46	9.7	0.91	32	15	2.1	Drained
4	1.47	9.5	0.91	32	14	2.3	Drained
5	1.47	9.5	0.91	33	33	1.0	Undrained
6	1.45	9.2	0.92	32	22	1.5	Undrained
7	1.48	9.4	0.91	33	18	1.8	Undrained

### Stress paths

The testing programme consisted of a series of drained triaxial tests, including multiple stress paths which allowed to explore different loading conditions, and a series of standard undrained triaxial compression tests. A saturation ramp by back pressure was performed up to a cell pressure  $\sigma_c = 200$  kPa. The cell pressure was then increased to 400 kPa under undrained conditions. To determine the volumetric response upon loading and unloading, sample 1 was isotropically compressed up to  $p'_0 = 74$  kPa (point b in Fig. 1a), and isotropically unloaded to  $p'_{\text{start shear}} = 18$  kPa, ending with  $\text{OCR} \cong 4$  (point c in Fig. 1a). The other samples were isotropically consolidated up to a mean effective stress  $p'_0 = 32 - 33$  kPa (Fig. 1a and Fig. 1b) and isotropically unloaded, to give an initial overconsolidation ratio  $\text{OCR} = p'_0 / p'_{\text{start shear}}$  between 1.0 and 2.3 depending on the test (Table 1). The initial preconsolidation pressure was decided in order to provide a representative data set in terms of stress levels for the typical field conditions of surficial peats in the Netherlands ( $\sigma'_v \cong 10 \div 40$  kPa). For the drained tests, the shearing stage consisted in a series of mixed isotropic and deviatoric loading - unloading and reloading paths, as

summarised in Fig. 1a and Fig. 1b. For sample 1 and sample 2 the deviatoric stress was increased at nominally constant  $p'$ , until the pre-defined stress ratios  $\eta = q/p'$ , equal to 1.92 and 0.78, respectively. For sample 3 and sample 4 multiple nominally constant  $p'$  and constant  $q$  traits were followed (note that the anticipated constant  $p'$  paths were not followed exactly due to difficulties in stress control). The remaining samples (5, 6 and 7) were brought to failure with a constant axial displacement rate of 0.02 mm/min and constant radial stress in undrained conditions.

The radial stress paths imposed to sample 1 and sample 2 were exploited to update the existing hypoplastic formulation (Fig. 1a). The remaining stress paths on sample 3 and sample 4 (Fig. 1b) together with the undrained tests were used to evaluate the model performance.

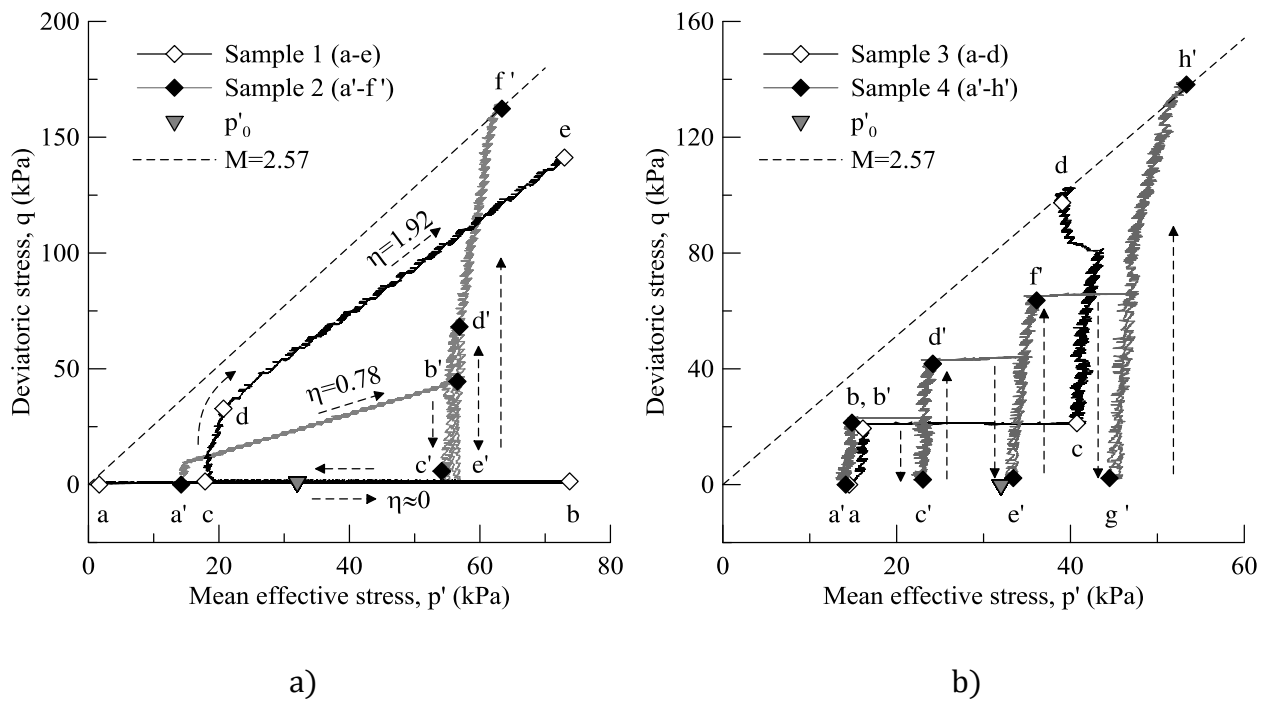


**Fig. 1** Experimental drained stress paths used for (a) model calibration and for (b) model assessment (the applied stress history can be followed through the letters in the figures)

The results in Fig. 1a and Fig. 1b show that failure was reached for a critical stress ratio  $M = 2.57$  corresponding to a critical friction angle  $\phi'_c = 64^\circ$ . Very high friction angles for peats are often

reported in the literature (Oikawa and Miyakawa [44]; Yamaguchi et al. [3]; Farrell and Hebib [4]; Cola and Cortellazzo [6]). However, the end restraint at the boundaries of the sample is likely to contribute to the observed high values (Rowe et al. [45]; Drescher and Vardoulakis [46]; Cheng et al. [7]). A dedicated experimental investigation to quantify this contribution is on-going (Muraro [47]).

## **HYPOPLASTIC FORMULATION**

To model the peat behaviour, the hypoplastic formulation proposed by Mašín [35], [36] was the starting point of this work. The main constitutive components are here recalled for the sake of clarity. The general non-linear hypoplastic formulation may be written as (Gudehus [48])

$$\overset{\circ}{\boldsymbol{\sigma}} = f_s \left( \mathbf{L} : \dot{\boldsymbol{\varepsilon}} + f_d \mathbf{N} \|\dot{\boldsymbol{\varepsilon}}\| \right) \quad (3)$$

Where  $\overset{\circ}{\boldsymbol{\sigma}}$  and  $\dot{\boldsymbol{\varepsilon}}$  represent the objective (Zaremba-Jaumann) stress rate and the Euler stretching tensor, respectively,  $\mathbf{L}$  and  $\mathbf{N}$  are fourth- and second- order constitutive tensors,  $f_s$  is the factor controlling the influence of mean stress (barotropy factor) and  $f_d$  is the factor controlling the influence of void ratio (pyknotropy factor). Eq. (3) was further developed by Mašín [35] allowing for the explicit incorporation of the asymptotic states. The complete set of equations of the final form employed in this study is given in the Appendix. The experimental programme allowed to investigate explicitly the asymptotic states of the tested peat in terms of state boundary surface and strain rate directions, as reported in the following paragraph.

## **MODEL CALIBRATION AND ENHANCEMENT**

The employed hypoplastic model had been originally proposed for fine-grained soils. As a consequence, the model parameters describing the asymptotic state boundary surface and the asymptotic strain rate directions had been validated for friction angles ranging between

$\varphi'_c = 20^\circ \div 35^\circ$ . Straightforward applicability of the original model to peats is not guaranteed due to their higher friction angle, and no application of this type of hypoplastic models has been reported so far.

Relevant drained stress paths from sample 1 and sample 2 (Fig. 1a) have been chosen to calibrate the constitutive formulation and to adapt some of its parts based on the experimental results.

Asymptotic states are defined as those states achieved by the soil after a sufficiently long proportional stretching with a constant direction of the strain rate. Conceptual representation of asymptotic states has been proposed by Gudehus [49] and Gudehus and Mašin [50]. For the case of radial compression stress paths at constant stress ratio, asymptotic states are traditionally defined as normal compression lines in the  $\ln(1+e)$ - $\ln p'/p'_r$  plane (Butterfield [51]), where  $p'_r$  is a reference stress which was chosen equal to 1 kPa. Fig. 2 reports the compression lines from sample 1 and sample 2 with the corresponding asymptotic states ( $\ln$  is the natural logarithm). Sample 1 was isotropically loaded and unloaded. After unloading, it was further compressed at constant  $p'$  and then loaded along a radial direction, having a constant stress ratio  $\eta = 1.92$ . Sample 2 was loaded along a radial direction having  $\eta = 0.78$  (see Fig. 1a).

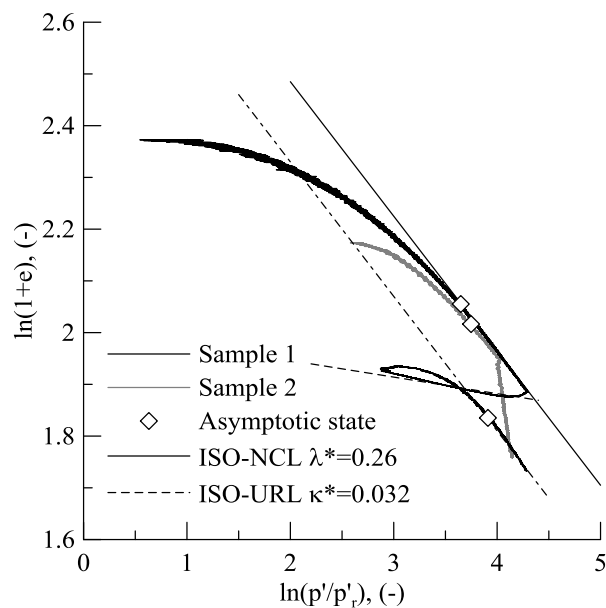


**Fig. 2** Radial paths data from sample 1 and sample 2 and the corresponding asymptotic states

The isotropic compression path and the isotropic unloading performed on the sample 1 (Fig. 1a) allow defining the ISO-NCL and the ISO-URL lines with  $\lambda^* = 0.26$  and  $\kappa^* = 0.032$ , respectively (Fig. 2). The asymptotic states lie on compression lines parallel to the ISO-NCL, as reported in Fig. 2. The critical stress ratio is fixed at  $\eta = M = 2.57$ , corresponding to a critical friction angle  $\varphi'_c = 64^\circ$ , from the failure line reached by sample 2 (Fig. 1a).

### Asymptotic state boundary surface

The envelope of all the asymptotic states in the stress versus void ratio space is defined as the asymptotic state boundary surface, ASBS, (Mašín and Herle [52]). The shape of its cross-section at constant void ratio is described from Mašín [35] by

$$f = 0 = F_m + \left( \frac{p'}{p'_e} \right)^\omega - 1 \quad (4)$$

where  $p'_e$  is the Hvorslev's equivalent pressure on the isotropic normal compression line, given by:

$$p'_e = p'_r \exp \left[ \frac{N - \ln(1 + e)}{\lambda^*} \right] \quad (5)$$

with  $N$  defining the position of the normal compression line.

The shape of the ASBS is controlled by the parameters  $\omega$  and  $a$ , according to

$$\omega = - \frac{\ln(\cos^2 \varphi'_c)}{\ln \vartheta_c^*} + a(F_m - \sin^2 \varphi'_c) \quad (6)$$

in which  $\vartheta_c^*$  defines the position of the critical state line on the ASBS and  $F_m$  is the Matsuoka-Nakai factor [53] defined as

$$F_m = \frac{9I_3 + I_1I_2}{I_3 + I_1I_2} \quad (7)$$

where  $I_1, I_2$  and  $I_3$  are the stress tensor invariants (recalled in the Appendix).

For the tested peat, the intersection of the ASBS with the critical state line occurs for  $\vartheta_c^* = p'_e/p'_{cr} = 2.2$  (with  $p'_{cr}$  the mean effective stress at critical state) slightly higher than the

original ratio of 2. Based on the asymptotic states and having fixed the critical state line, the final shape of the ASBS is reported in Fig. 3. The formulation ensures that the ASBS respects the tension cut off line for  $\eta = 3$ .

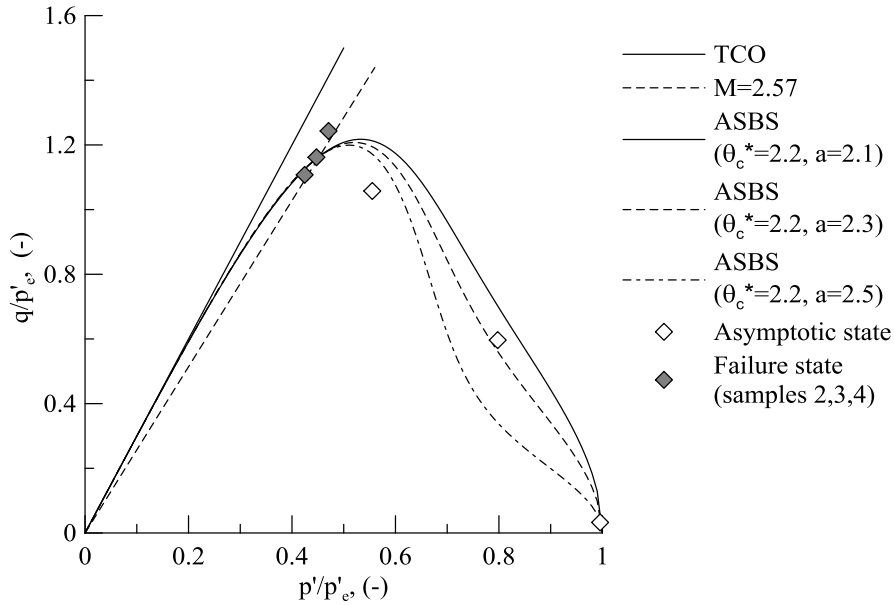


**Fig. 3** Asymptotic state boundary surface used in the model compared to the experimental data

The ASBS can assume unrealistic shapes for high value of the parameter  $a$  in eq. (6) as displayed in Fig. 3. Despite this problem not limiting the applicability of hypoplastic formulations, the loss of convexity of the ASBS is not supported by any experimental evidence. To limit this problem, and at the same time keeping a good match with the experimental data, a value  $a = 2.1$  was assumed.

### Asymptotic strain rate direction

The asymptotic behaviour of soils can be described in terms of relationship between proportional deformation paths and the corresponding asymptotic stress states. With reference to Fig. 4a and Fig. 4b, it is convenient to represent the strain rate obliquity and the stress obliquity with respect to the isotropic stress-strain state through the two angles  $\psi_{\dot{\epsilon}}$  and  $\psi_{\sigma'}$ , respectively. Relevant

deformation paths on the  $\dot{\epsilon}_a - \sqrt{2}\dot{\epsilon}_r$  plane and the corresponding asymptotic stress states on the Rendulic stress space  $\sigma'_a - \sqrt{2}\sigma'_r$  are reported in Table 2 and in Fig. 5.

**Table 2** Values of the angles  $\psi_{\dot{\epsilon}}$  and  $\psi_{\sigma'}$  at relevant states

State		Condition	$\psi_{\dot{\epsilon}}$ [°]	$\psi_{\sigma'}$ [°]
Isotropic compression	i	$\dot{\epsilon}_a = \dot{\epsilon}_r$	0	0
Isochoric compression (critical state)	c	$\dot{\epsilon}_p = 0$	90	$\tan^{-1}\left(\frac{2\sqrt{2}\sin\varphi'_c}{3 - \sin\varphi'_c}\right)$
Isochoric extension (critical state)	-c	$\dot{\epsilon}_p = 0$	-90	$-\tan^{-1}\left(\frac{2\sqrt{2}\sin\varphi'_c}{3 + \sin\varphi'_c}\right)$
Axial splitting (Tension cut off line)	d	$\dot{\epsilon}_a = 0$ $\sigma'_r = 0$	144.7	54.7
Discing	-d	$\dot{\epsilon}_r = 0$ $\sigma'_a = 0$	-125.3	-35.3

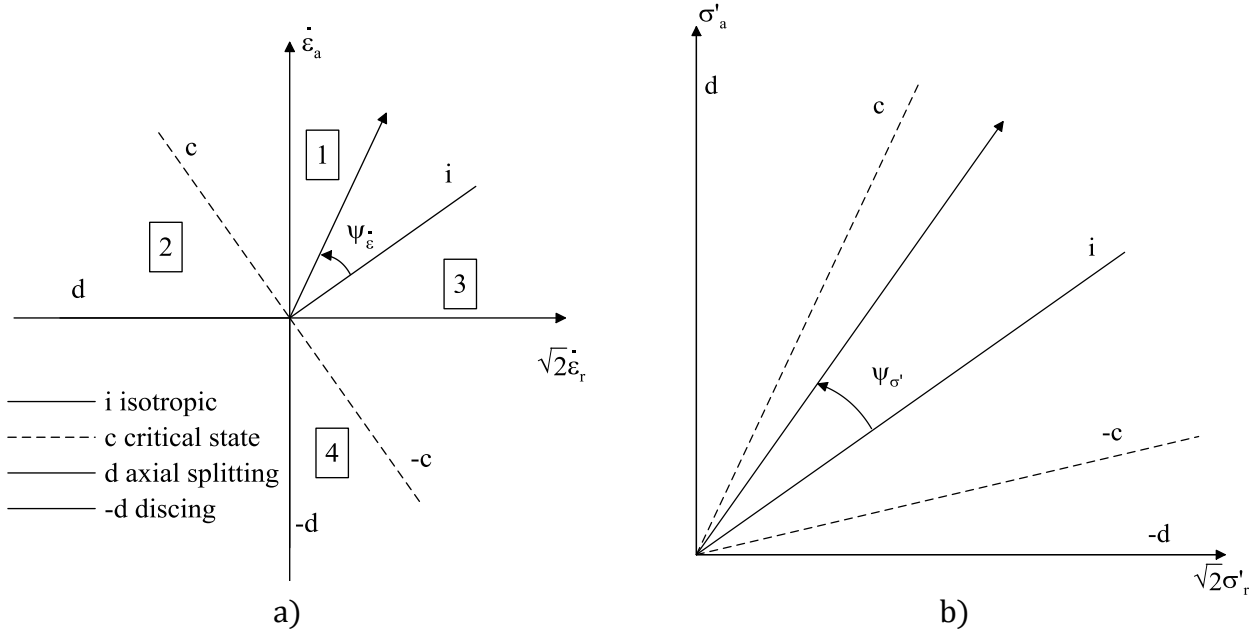


**Fig. 4** Definition of the angles  $\psi_\varepsilon$  (a) and (b)  $\psi_{\sigma'}$

The asymptotic strain rate direction  $\mathbf{d}$  is calculated as

$$\mathbf{d} = \frac{\mathbf{d}^A}{\|\mathbf{d}^A\|} \quad (8)$$

where

$$\mathbf{d}^A = -\hat{\boldsymbol{\sigma}}^* + \mathbf{1} \left[ \frac{2}{3} - \frac{\cos 3\theta + 1}{4} (F_m)^{1/4} \right] \frac{(F_m)^{\xi/2} - \sin^\xi \varphi'_c}{1 - \sin^\xi \varphi'_c} \quad (9)$$

with  $\theta$  the Lode's angle and  $\hat{\boldsymbol{\sigma}}^*$  the normalised deviatoric stress (for the definition, see the Appendix).

The coefficient  $\xi$  in eq. (9) controls the asymptotic strain rate direction, and was originally defined by Mašín [35] as

$$\xi = 1.7 + 3.9 \sin^2 \varphi'_c \quad (10)$$

The asymptotic strain rate direction predicted by the original model (Mašín [35]) is exemplified in Fig. 5 in terms of the  $\psi_{\sigma'} - \psi_\varepsilon$  relationship for a value of the critical friction angle  $\varphi'_c = 30^\circ$ .

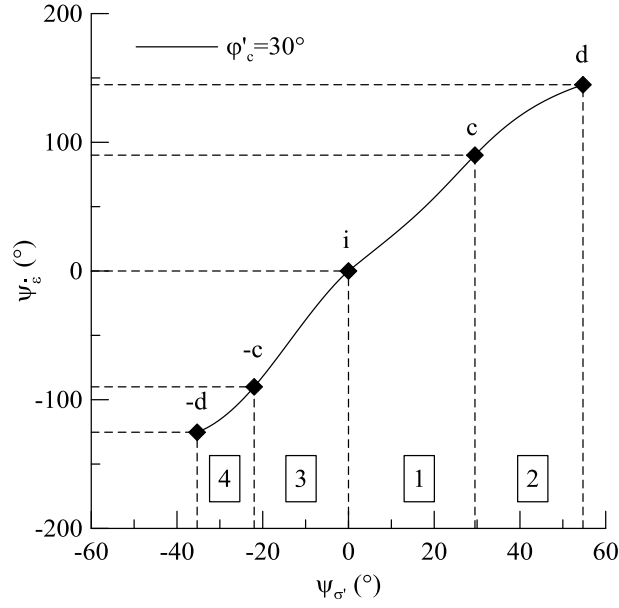


**Fig. 5** Graphical representation of the asymptotic strain rate direction with the corresponding relevant states for  $\varphi'_c = 30^\circ$

The experimental asymptotic strain rate direction (ASRD) for the tested peat has been computed from the asymptotic states defined in Fig. 2 for each radial stress path. To allow proper representation of the experimental data, the original model in Mašin [35] (eq. (10)) had to be modified through a coefficient  $\xi$  in eq. (9) as

$$\xi = \xi^\zeta \quad (11)$$

where the exponent  $\zeta$  was assumed equal to 1.8 in order to fit the experimental data. The coefficient  $\xi$  rules the ratio between the deviatoric and the volumetric strain along any stress path. The adopted  $\zeta$  higher than 1 increases the deviatoric strain increment for the same imposed stress ratio compared to the original model (eq. (10)). Fig. 6 shows the predicted values for the original expression in Mašin [35] and the one adopted in this study (eq. (11)) together with the experimental results. For the sake of comparison, the corresponding curves for the Original Cam clay (OCC, Roscoe et al. [54]) and the Modified Cam clay (MCC, Roscoe and Burland [23]) models are plotted too. It is worth noting that the last two models do not respect the limitation imposed by the tension

cut-off line, differently from the original and the proposed hypoplastic formulations.

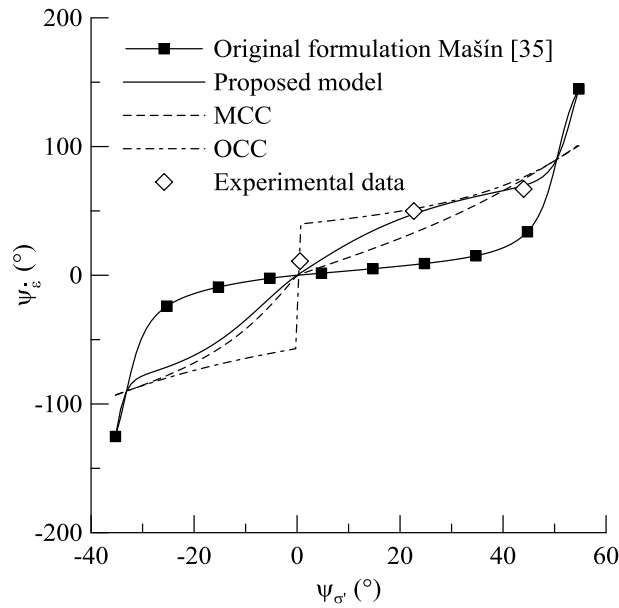


**Fig. 6** Asymptotic strain rate direction for the proposed and original model compared with the experimental results

Significant improvement is obtained by adopting the eq. (11) for the asymptotic strain rate direction with respect to the original hypoplastic formulation, eq. (10), which was calibrated on clays. Having defined the asymptotic states through the ASBS and the ASRD, the hypoplastic model requires the calibration of the 5 basic parameters:  $\varphi'_c$ ,  $\lambda^*$ ,  $\kappa^*$ ,  $N$ ,  $\nu$  and of the additional parameters  $\vartheta_c^*$ ,  $\zeta$  and  $\alpha_f$  (see the Appendix).

## MODEL RESULTS

The capabilities of the model have been tested in two steps. Firstly, the multiple stress paths performed on sample 1 and sample 2, other than the radial paths on which the asymptotic states had been determined, have been simulated to validate the formulation. Secondly, the model predictions have been compared to the experimental data from the other tested samples. The parameters used in

the simulations are summarised in Table 3. A constant value of the parameter  $\alpha_f = 2$  has been used (instead of eq. (21) in the Appendix) as in Mašin [35].

**Table 3** Parameters of the model used in the simulations

$\varphi'_c$	$\lambda^*$	$\kappa^*$	N	$\nu$	$\vartheta_c^*$	$\zeta$	$\alpha_f$
64°	0.26	0.032	3.005	0.2	2.2	1.8	2.0

It is worth noting that in hypoplasticity the value of  $\kappa^*$  represents the initial slope of the unloading line in the  $\ln(1 + e)$ - $\ln p'/p'_r$  plane upon unloading from the normally consolidated state. However, contrarily to classic elasto-plasticity, the response is non-reversible inside the ASBS and the slope of the unloading line does not exactly correspond to  $\kappa^*$ . The value of  $\kappa^*$  adopted in the simulations (Table 3) was thus calibrated back-analysing the results of the isotropic unloading path on sample 1 (Fig. 2).

### Model performance

Simulations of the entire stress paths from sample 1 and sample 2 are shown in Fig. 7 and Fig. 8. The radial stress paths in Fig. 7a and Fig 8a were used to define the asymptotic states, which implies the very good agreement between the experimental data and the model simulations. The agreement is also quite good on the subsequent stress paths, involving different deviatoric stresses. Over the final portion of the test, the model appears to respond stiffer than the soil tested. In general, the hypoplastic formulation allows a satisfactory prediction of the pre-failure behaviour over various loading directions.

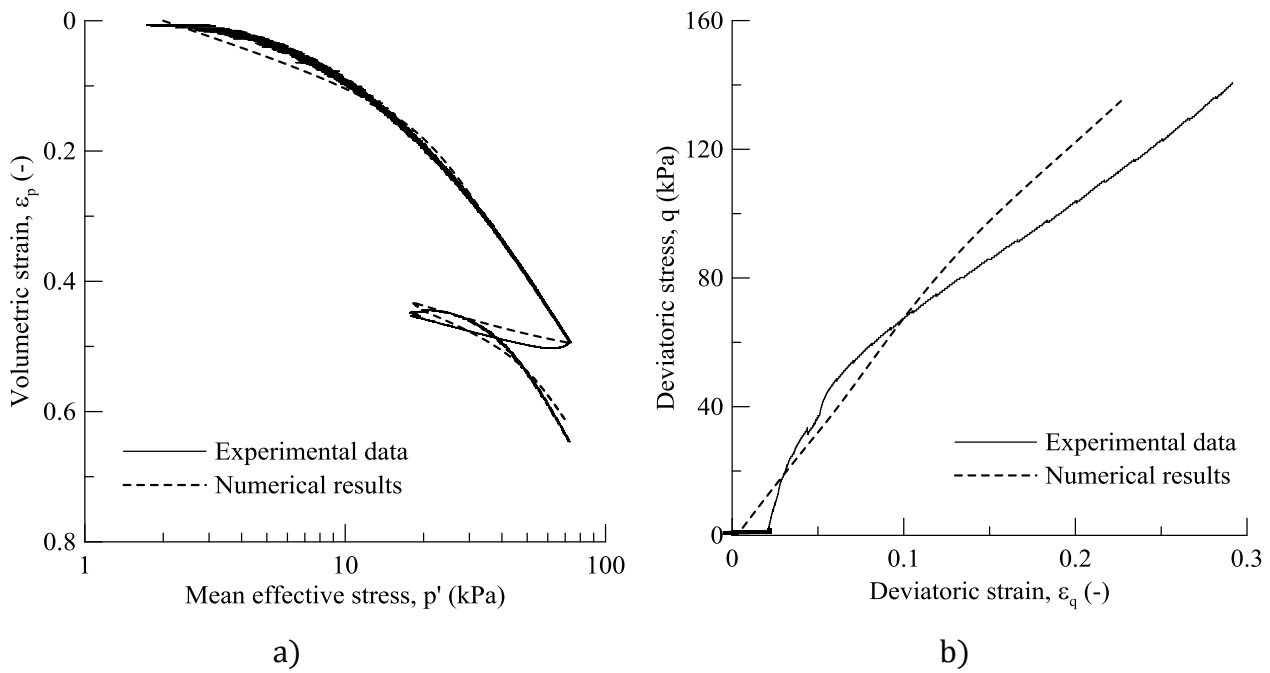


**Fig. 7** Comparison between the experimental results and the model simulation for sample 1 in terms of (a) volumetric response ( $p' - \epsilon_p$ ) and (b) deviatoric response ( $q - \epsilon_q$ )

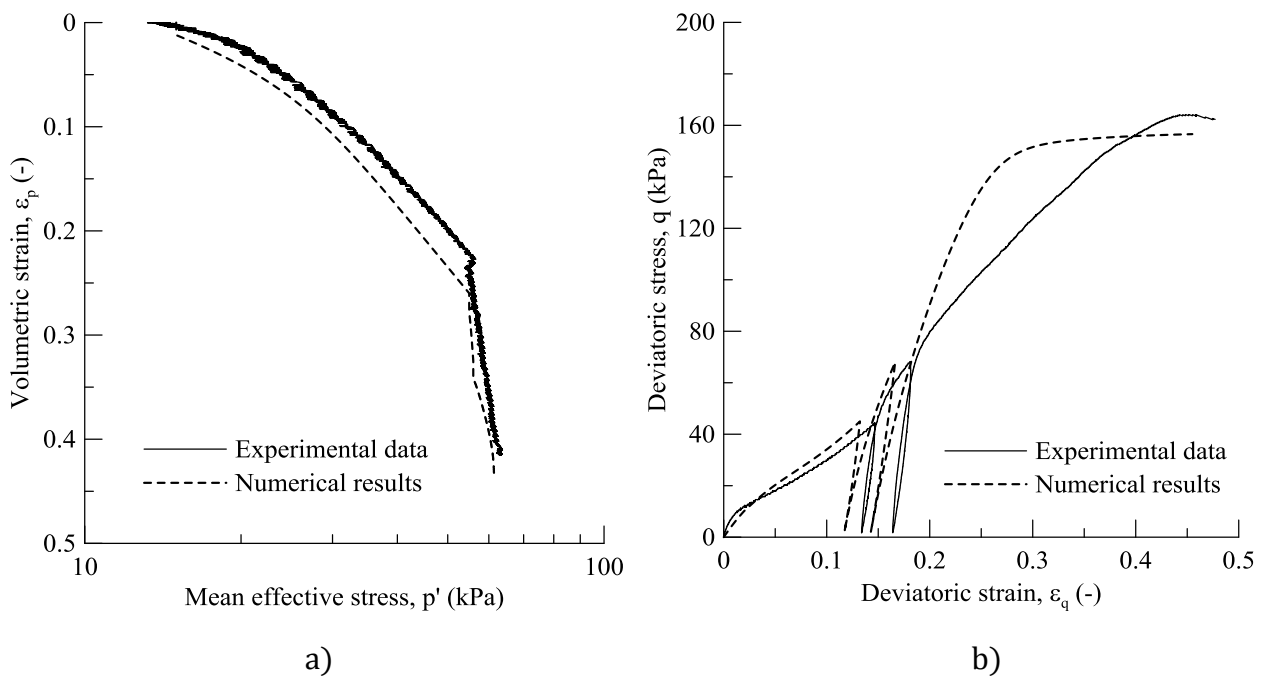


**Fig. 8** Comparison between the experimental results and the model simulation for sample 2 in terms of (a) volumetric response ( $p' - \epsilon_p$ ) and (b) deviatoric response ( $q - \epsilon_q$ )

The underestimation of the deviatoric strain for a given deviatoric stress increases with the strain level. Furthermore, the hysteric behaviour observed in the experimental tests with cycles of isotropic (Fig. 7a) and deviatoric loading and unloading (Fig. 8b) is not properly captured by the adopted model. Intergranular strain concept developed by Niemunis and Herle [55] could be introduced to account for this effect, but this is out of the primary scope of this paper.

## Model predictions

### - Drained triaxial tests

To further test the model capabilities, the results of the tests on sample 3 and sample 4 are analysed, where complex stress conditions have been applied with multiples traits of volumetric and deviatoric stress paths.

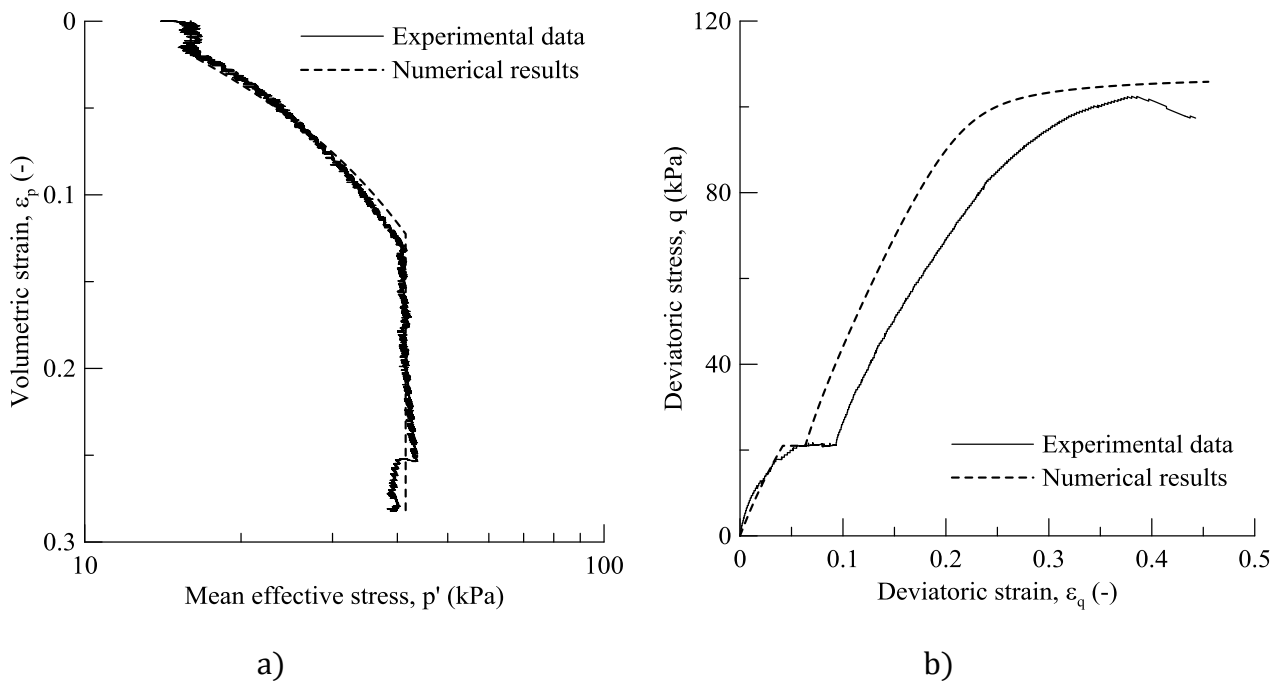


**Fig. 9** Comparison between the experimental results and the model simulation for sample 3 in terms of (a) volumetric response ( $p' - \epsilon_p$ ) and (b) deviatoric response ( $q - \epsilon_q$ )

The comparisons in Fig. 9 and Fig. 10 confirm the previous considerations, with good agreement on the volumetric stress-strain response and less satisfactory simulation of the deviatoric response for high strain levels. The limitations of the adopted model in describing the cyclic response are magnified by the comparison on sample 4, with multiple cycles of deviatoric unloading-reloading.

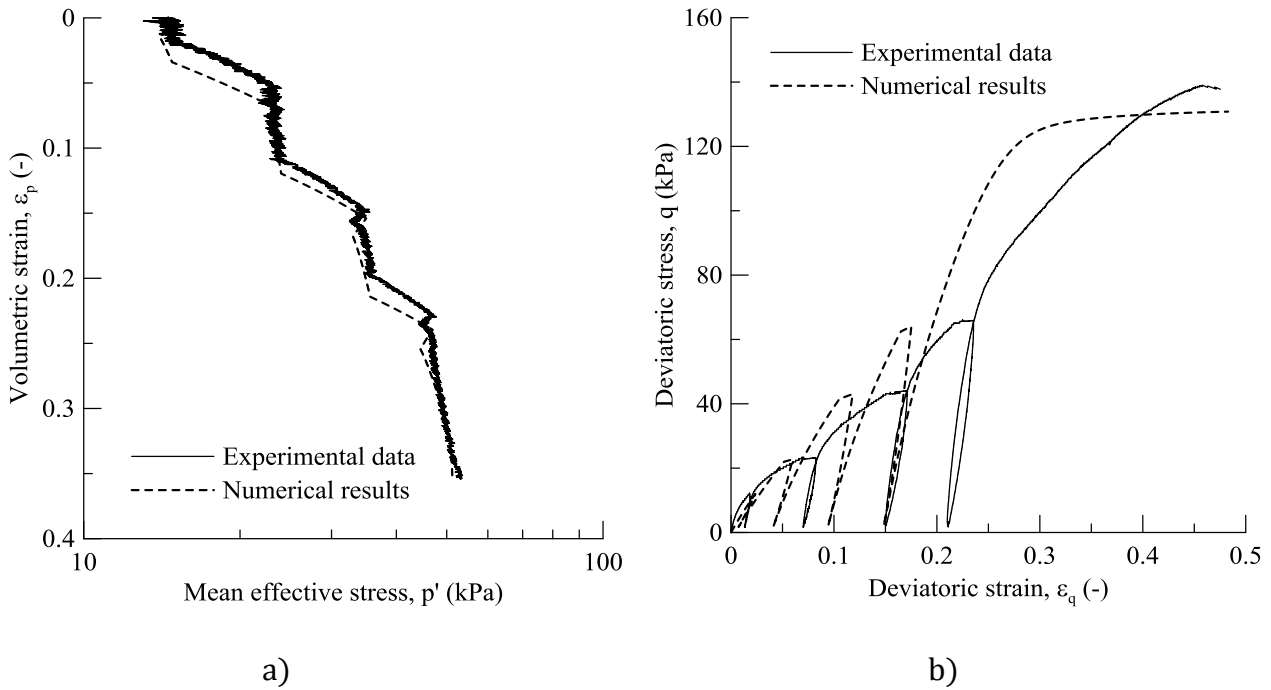


**Fig. 10** Comparison between the experimental results and the model simulation for sample 4 in terms of (a) volumetric response ( $p' - \epsilon_p$ ) and (b) deviatoric response ( $q - \epsilon_q$ )

The experimental stress-dilatancy relationship is compared with the model prediction for non-proportional deformation paths in Fig. 11. Different non-proportional stress paths are considered. Fig. 11a reports the comparison between the experimental data and the model prediction on the last  $p'$  constant trait applied to the sample 2, while Fig. 11b shows the same for the  $q$  constant and the  $p'$  constant traits for sample 3. Following the hypoplastic approach, the strain increment direction is defined in terms of total strain increments (and not in plastic strain increments as in elastic-plastic models) as

$$\tan \beta = \frac{\delta \varepsilon_q}{\delta \varepsilon_p} \quad (12)$$

where the  $\delta \varepsilon_q$  and  $\delta \varepsilon_p$  are the increment in the deviatoric and volumetric strains, respectively.

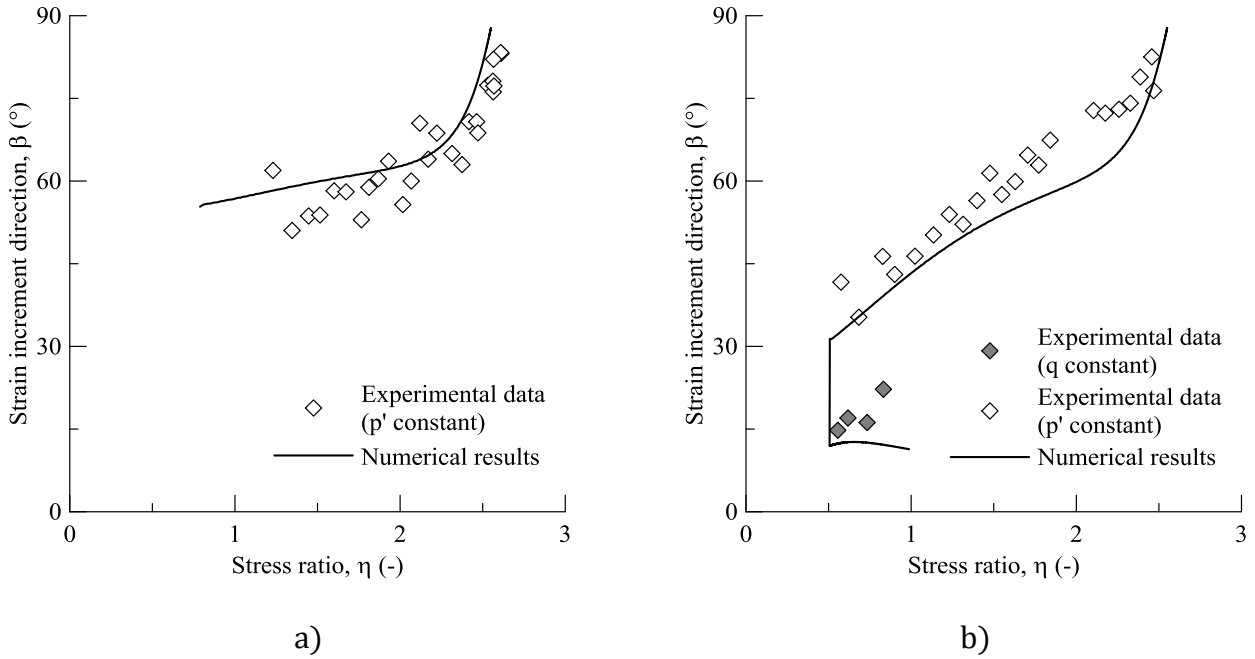


**Fig. 11** Strain increment direction obtained from multiple stress paths from sample 2 (a) and from sample 3 (b) compared to the model simulation

The adopted asymptotic strain rate direction relationship (Fig. 6) well matches the experimental results even for non-proportional strain paths as the ones in Fig. 11a and Fig. 11b, and supports the adoption of the hypoplastic formulation for peat behaviour under complex loading conditions.

### - Undrained triaxial compression tests

The model capabilities are further tested against the experimental results from undrained triaxial compression tests performed on sample 5, sample 6 and sample 7, for three different values of OCR. The numerical predictions are compared with the experimental data in Fig. 12 in terms of

stress-path and deviatoric stress-strain response. It is worth noting that the samples tested in undrained conditions, failed at a stress ratio slightly lower than the one reached in drained compression. This difference, already observed in Zhang and O’Kelly [56], is most probably due to the different geometrical constraints imposed in the two types of tests (Drescher and Vardoulakis [46]; Muraro [47]).

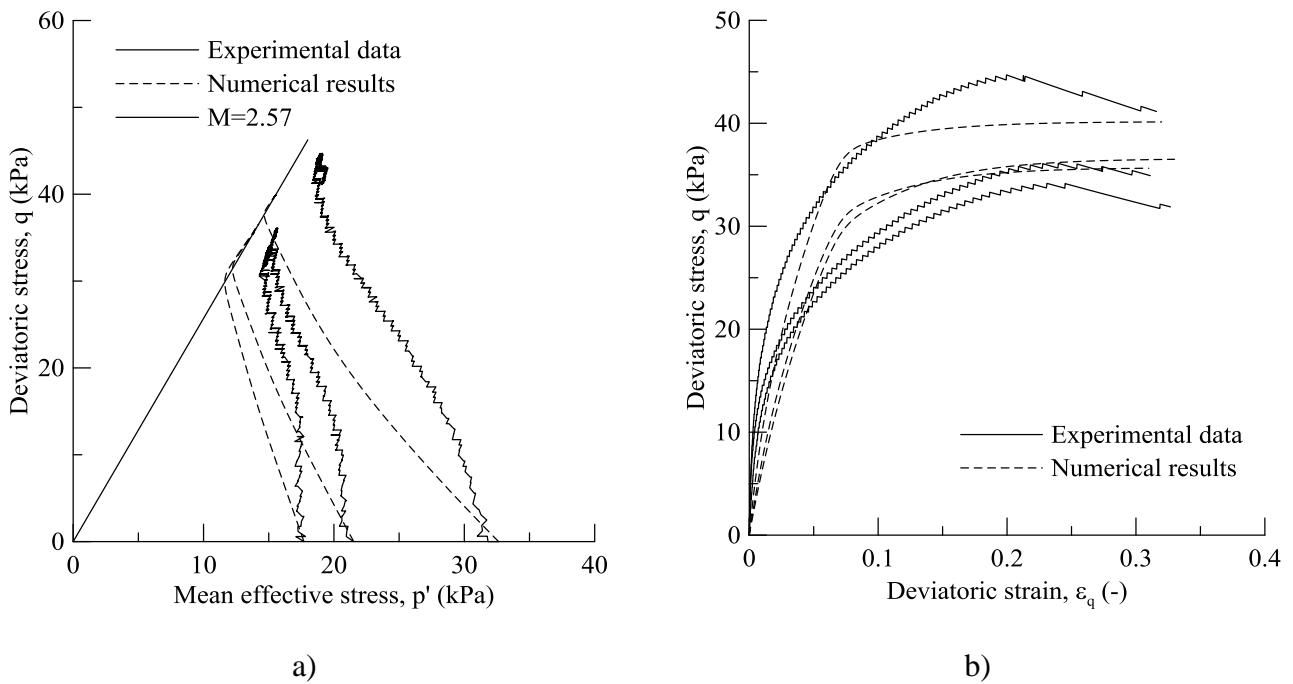


**Fig. 12** Comparison between the experimental results and the model simulation for sample 5, 6 and 7 in terms of (a) stress path and (b) deviatoric response ( $q - \epsilon_q$ )

The agreement between the stress - strain curve is qualitatively good. However, the model does not properly represent the initial slope of the stress path in  $p'$  -  $q$  plane. This shortcoming can be eliminated by adopting approach from Mašín and Herle [57], which is outside the scope of the present paper.

## CONCLUDING REMARKS

A first attempt of modelling the behaviour of reconstituted peat in the framework of hypoplasticity has been proposed. The formulation is based on an existing model originally developed for clays, which has been adapted to properly account for the peculiar characteristics of peat: a material with an extremely high compressibility and exceptionally high friction angle. An advanced laboratory investigation was carried out to define explicitly the constitutive ingredients of the hypoplastic model. Non-standard drained triaxial compression tests were chosen, in which multiple stress paths were applied to the samples, allowing to validate the adopted model on a variety of loading directions. The results confirm the capability of hypoplasticity to capture fundamental aspects of the pre-failure behaviour of peats such as the non-linearity inside the state boundary surface and the directional response. The model represents a robust base suitable for further developments and enhancements, such as introduction of anisotropy and creep.

The modelling exercise highlights that peats behave differently from clays, although they are frequently associated into the broad category of “soft soils”. Both the shape of the ASBS and the ASRD indicate a predominant role of the deviatoric stress-strain components on the yielding of peats compared with their volumetric counterparts, which distinguish the behaviour of peats from that of clays.

## APPENDIX

The entire set of equations needed in the model formulation is listed herein. Further details are reported in Mašin [35], [36].

$$\overset{\circ}{\boldsymbol{\sigma}} = f_s \mathbf{L} : \dot{\boldsymbol{\varepsilon}} - \frac{f_d}{f_d^A} \mathbf{A} : \mathbf{d} \|\dot{\boldsymbol{\varepsilon}}\| \quad (13)$$

with

$$\mathbf{L} = \mathbf{I} + \frac{\nu}{1 - 2\nu} \mathbf{1} \otimes \mathbf{1} \quad (14)$$

$$\mathbf{A} = f_s \mathbf{L} + \frac{\boldsymbol{\sigma}}{\lambda^*} \otimes \mathbf{1} \quad (15)$$

$$f_d = \left( \frac{\vartheta_c^* p'}{p'_e} \right)^{\alpha_f} \quad (16)$$

$$f_s = \frac{3p'}{2} \left( \frac{1}{\lambda^*} + \frac{1}{\kappa^*} \right) \frac{1 - 2\nu}{1 + \nu} \quad (17)$$

$$p'_e = p'_r \exp \left[ \frac{N - \ln(1 + e)}{\lambda^*} \right] \quad (18)$$

where  $\mathbf{1}$  and  $\mathbf{I}$  are the second and the fourth order unity tensors,  $\lambda^*$  is the slope of the isotropic normally consolidated line,  $\kappa^*$  is the slope of the isotropic unloading line for unloading starting from the isotropic normally consolidated state and  $\nu$  is the parameter controlling the proportion of bulk and shear stiffness.  $p'_e$  is the Hvorslev's equivalent pressure on the isotropic normal compression line with  $N$  defining the position of the normal compression line and  $p'_r$  is a reference pressure of 1 kPa.

The position of the critical state line on the asymptotic state boundary surface (ASBS) is specified as in Ragni et al. [58] through

$$\frac{p'_e}{p'_{cr}} = \vartheta_c^* \quad (19)$$

Note that for  $\vartheta_c^* = 2$  the original model is recovered.

The non-linear response inside the ASBS is governed by the factor  $f_d$ . The value  $f_d^A$  needed in eq. (13) is computed by combining eq. (16) with the explicit ASBS formulation to give

$$f_d^A = \vartheta_c^{*\alpha_f} (1 - F_m)^{\alpha_f/\omega} \quad (20)$$

where  $\alpha_f$  can be considered as a model parameter controlling the non-linear response inside the asymptotic state boundary surface. Mašín and Herle [52] and Mašín [36] suggested

$$\alpha_f = \frac{\ln \left[ \frac{\lambda^* - \kappa^* \left( \frac{3 + a_f^2}{a_f \sqrt{3}} \right)}{\lambda^* + \kappa^* \left( \frac{3 + a_f^2}{a_f \sqrt{3}} \right)} \right]}{\ln \vartheta_c^*} \quad (21)$$

$$a_f = \frac{\sqrt{3}(3 - \sin \varphi'_c)}{2\sqrt{2} \sin \varphi'_c} \quad (22)$$

The shape of the ASBS is controlled by the parameters  $\omega$

$$\omega = -\frac{\ln(\cos^2 \varphi'_c)}{\ln \vartheta_c^*} + a(F_m - \sin^2 \varphi'_c) \quad (23)$$

with  $a = 2.1$  for the case of the tested peat and with  $F_m$  the Matsuoka-Nakai factor defined as

$$F_m = \frac{9I_3 + I_1 I_2}{I_3 + I_1 I_2} \quad (24)$$

The stress invariants are defined as

$$I_1 = \text{tr} \boldsymbol{\sigma} \quad (25)$$

$$I_2 = \frac{1}{2} [\boldsymbol{\sigma} : \boldsymbol{\sigma} - (I_1)^2] \quad (26)$$

$$I_3 = \det \boldsymbol{\sigma} \quad (27)$$

Finally, the asymptotic strain rate direction  $\mathbf{d}$  is calculated as

$$\mathbf{d} = \frac{\mathbf{d}^A}{\|\mathbf{d}^A\|} \quad (28)$$

where

$$\mathbf{d}^A = -\hat{\boldsymbol{\sigma}}^* + \mathbf{1} \left[ \frac{2}{3} - \frac{\cos 3\theta + 1}{4} (F_m)^{1/4} \right] \frac{(F_m)^{\xi/2} - \sin^\xi \varphi'_c}{1 - \sin^\xi \varphi'_c} \quad (29)$$

with  $\theta$  the Lode's angle and  $\hat{\boldsymbol{\sigma}}^*$  the normalised deviatoric stress defined as

$$\cos 3\theta = -\sqrt{6} \frac{\text{tr}(\hat{\boldsymbol{\sigma}}^* \cdot \hat{\boldsymbol{\sigma}}^* \cdot \hat{\boldsymbol{\sigma}}^*)}{[\hat{\boldsymbol{\sigma}}^* : \hat{\boldsymbol{\sigma}}^*]^{3/2}} \quad (30)$$

$$\hat{\boldsymbol{\sigma}}^* = \frac{\boldsymbol{\sigma}}{\text{tr} \boldsymbol{\sigma}} - \frac{\mathbf{1}}{3} \quad (31)$$

The coefficient  $\xi$  in eq. (29), originally defined by Mašín [35], has been modified by introducing the exponent  $\zeta$  equals to 1.8 based on the experimental results

$$\xi = (1.7 + 3.9 \sin^2 \varphi'_c)^\zeta \quad (32)$$

## ACKNOWLEDGEMENT

The financial support of the Dutch Organisation for Scientific Research (NWO), under the project “Reliability-Based Geomechanical Assessment Tools for Dykes and Embankments in Delta Areas - 13864 (Reliable Dykes)” is gratefully acknowledged. The financial support from the

Charles University mobility fund is gratefully acknowledged. The second author is grateful for the institutional support by Center for Geosphere Dynamics (UNCE/SCI/006).

## REFERENCES

- [1] Adams JI. Laboratory compression tests on peat. 7th Muskeg Research Conference. Ottawa: NCR, ACSSM Technical Memorandum 1961; 71:36–54.
- [2] Landva AO, La Rochelle P. Compressibility and shear characteristics of Radforth peats. Testing of peats and organic soils: ASTM International 1983; 157-191.
- [3] Yamaguchi H, Ohira Y, Kogure K, Mori S. Undrained shear characteristics of normally consolidated peat under triaxial compression and extension conditions. *Soils and Foundations* 1985; 25(3):1-18.
- [4] Farrell ER, Hebib S. The determination of the geotechnical parameters of organic soils. In: *Proceedings of International Symposium on problematic soil* (Moroto N, Mitachi T eds) 1998; 33-36.
- [5] Edil TB, Wang X. Shear strength and  $K_0$  of peats and organic soils. *Geotechnics of high water content materials*: ASTM International 2000; 209-226.
- [6] Cola S, Cortellazzo G. The shear strength behavior of two peaty soils. *Geotechnical and Geological Engineering* 2005; 23(6):679-695.
- [7] Cheng XH, Ngan-Tillard DJM, Den Haan EJ. The causes of the high friction angle of Dutch organic soils. *Engineering geology* 2007; 93(1):31-44.
- [8] Berry PL, Poskitt TJ. The consolidation of peat. *Géotechnique* 1972; 22(1):27-52.
- [9] Berry PL, Vickers B. Consolidation of fibrous peat. *Journal of the Geotechnical Engineering Division* 1975; 101(8):741-753.
- [10] Lefebvre G, Langlois P, Lupien C, Lavallée JG. Laboratory testing and in situ behaviour of peat as embankment foundation. *Canadian Geotechnical Journal* 1984; 21(2):322-337.
- [11] Tsushima M. Experimental study on creep rupture characteristics of Peat. *Soils and foundations* 1985; 25(1):137-141.
- [12] Fox PJ, Edil TB, Lan LT.  $C_a/C_c$  concept applied to compression of peat. *Journal of geotechnical engineering* 1992; 118(8):1256-1263.
- [13] Edil TB, Fox PJ, Lan LT. Stress-induced one-dimensional creep of peat. In: *Advances in Understanding and Modelling the Mechanical Behaviour of Peat* (Den Haan EJ, Termaat R, Edil TB, eds). Delft: Balkema, Rotterdam 1994; 3-18.
- [14] Fox PJ, Edil TB. Effects of stress and temperature on secondary compression of peat. *Canadian Geotechnical Journal* 1996; 33(3):405-415.

- [15] Den Haan EJ, Edil TB. Secondary and tertiary compression of peat. In: *Advances in Understanding and Modelling the Mechanical Behaviour of Peat* (Den Haan EJ, Termaat R, Edil TB, eds) 1994; 49-60.
- [16] Mesri G, Stark TD, Ajlouni MA, Chen CS. Secondary compression of peat with or without surcharging. *Journal of Geotechnical and Geoenvironmental Engineering* 1997; 123(5):411-421.
- [17] Den Haan EJ, Kruse GAM. Characterisation and engineering properties of Dutch peats. *Proceedings of the Second International Workshop of Characterisation and Engineering Properties of Natural Soils Singapore* 2007; 2101-2133.
- [18] Mesri G, Ajlouni M. Engineering properties of fibrous peats. *Journal of Geotechnical and Geoenvironmental Engineering* 2007; 133(7):850-866.
- [19] Madaschi A, Gajo A. One-dimensional response of peaty soils subjected to a wide range of oedometric conditions. *Géotechnique* 2015; 65(4):274-286.
- [20] Acharya MP, Hendry MT, Martin CD. Creep behaviour of intact and remoulded fibrous peat. *Acta Geotechnica* 2017; 13(2):399-417.
- [21] Den Haan EJ. A compression model for non-brittle soft clays and peat. *Géotechnique* 1996; 46(1):1-16.
- [22] Madaschi A, Gajo A. Constitutive modelling of viscous behaviour of soils: A case study. *Geomechanics for Energy and the Environment* 2015; 4:39-50.
- [23] Roscoe KH, Burland JB. On the generalized stress-strain behaviour of wet clay. In: *Engineering plasticity* (Heyman J, Leckie FA, eds). Cambridge: Cambridge University Press 1968; 535-609.
- [24] Den Haan EJ, Feddema A. Deformation and strength of embankments on soft Dutch soil. *Proceedings of the Institution of Civil Engineers-Geotechnical engineering* 2013; 166(3):239-252.
- [25] Den Haan EJ. Modelling peat with an anisotropic time-dependent model for clay. In: *Numerical Methods in Geotechnical Engineering: Taylor and Francis Group* (Hicks MA, Brinkgreve RBJ, Rohe A, eds) 2014; 55-60.
- [26] Leoni M, Karstunen M, Vermeer P. Anisotropic creep model for soft soils. *Géotechnique* 2008; 58(3):215-226.
- [27] Vermeer PA, Neher HP. A soft soil model that accounts for creep. In: *Proceedings of the international symposium Beyond 2000 in Computational Geotechnics* (Brinkgreve RBJ, ed) Balkema, Rotterdam 1999; 249-261.
- [28] Wheeler SJ, Näätänen A, Karstunen M, Lojander M. An anisotropic elastoplastic model for soft clays. *Canadian Geotechnical Journal* 2003; 40(2):403-418.
- [29] Boumezerane D. Modeling unloading/reloading in peat using a kinematic bubble model. In: *Numerical Methods in Geotechnical Engineering: Taylor and Francis Group* (Hicks MA, Brinkgreve RBJ, Rohe A, eds) 2014; 9-14.

- [30] Al-Tabbaa A, Wood DM. An experimentally based 'bubble' model for clay. Proceedings of the 3rd International Symposium on Numerical Models in Geomechanics NUMOG III: Elsevier Applied Science 1989; 91-99.
- [31] Sivasithamparam N. Development and implementation of advanced soft soil models in finite elements. PhD thesis: University of Strathclyde; 2012.
- [32] Yang ZX, Zhao CF, Xu CJ, Wilkinson SP, Cai YQ, Pan K. Modelling the engineering behaviour of fibrous peat formed due to rapid anthropogenic terrestrialization in Hangzhou, China. *Engineering Geology* 2016; 215:25-35.
- [33] Li XS, Dafalias YF. Dilatancy for cohesionless soils. *Géotechnique* 2000; 50(4):449-460.
- [34] Boumezerane D, Makdisi A, Grimstad G. A framework for peat behaviour based on hyperplasticity principles. *Creep and Deformation Characteristics in Geomaterials*. Gothenburg, Sweden 2015; 1-4.
- [35] Mašin D. Clay hypoplasticity with explicitly defined asymptotic states. *Acta Geotechnica* 2013; 8(5):481-496.
- [36] Mašin D. Clay hypoplasticity model including stiffness anisotropy. *Géotechnique* 2014; 64(3):232-238.
- [37] Ludwik P. *Elemente der technologischen Mechanik*: Springer-Verlag; 1909.
- [38] Hencky H. Über die Form des Elastizitätsgesetzes bei ideal elastischen Stoffen. *Zeitschrift für technische Physik* 1928; 6:215-220.
- [39] Head KH, Epps RJ. *Manual of soil laboratory testing – Vol. III: Effective stress tests*. Dunbeath, UK: Whitteles Publishing; 2014.
- [40] Head KH. *Manual of soil laboratory testing – Vol. I: Soil classification and compaction tests*. Dunbeath, UK: Whitteles Publishing; 2014.
- [41] D5550-14A. Standard test method for specific gravity of soil solids by gas pycnometer. American Society of Testing and Materials; 2014.
- [42] D2974-14A. Standard test methods for moisture, ash, and organic matter of peat and other organic soils. American Society of Testing and Materials; 2014.
- [43] D1997-13A. Standard test method for laboratory determination of the fiber content of peat samples by dry mass. American Society of Testing and Materials; 2013.
- [44] Oikawa H, Miyakawa I. Undrained shear characteristics of peat. *Soils and foundations* 1980; 20(3):91-100.
- [45] Rowe RK, MacLean MD, Soderman KL. Analysis of a geotextile-reinforced embankment constructed on peat. *Canadian Geotechnical Journal* 1984; 21(3):563-576.
- [46] Drescher A, Vardoulakis I. Geometric softening in triaxial tests on granular material. *Géotechnique* 1982;32(4):291-303.

- [47] Muraro S. Hydro-mechanical behaviour of peat. PhD thesis, under preparation: Delft University of Technology; 2018.
- [48] Gudehus G. A comprehensive constitutive equation for granular materials. *Soils and foundations* 1996; 36(1):1-12.
- [49] Gudehus G. *Physical soil mechanics*: Springer Science & Business Media; 2011.
- [50] Gudehus G, Mašín D. Graphical representation of constitutive equations. *Géotechnique* 2009; 59(2):147-151.
- [51] Butterfield R. A natural compression law for soils. *Géotechnique* 1979; 29(4):469-480.
- [52] Mašín D, Herle I. State boundary surface of a hypoplastic model for clays. *Computers and Geotechnics* 2005; 32(6):400-410.
- [53] Matsuoka H, Nakai T. Stress-deformation and strength characteristics of soil under three different principal stresses. *Proceedings of the Japan Society of Civil Engineers: Japan Society of Civil Engineers* 1974; 59-70.
- [54] Roscoe KH, Schofield AN, Thurairajah A. Yielding of clays in states wetter than critical. *Géotechnique* 1963; 13(3):211-240.
- [55] Niemunis A, Herle I. Hypoplastic model for cohesionless soils with elastic strain range. *Mechanics of Cohesive Frictional Materials* 1997;2(4):279-299.
- [56] Zhang L, O'Kelly BC. The principle of effective stress and triaxial compression testing of peat. *Proceedings of the Institution of Civil Engineers-Geotechnical Engineering* 2014;167(1):40-50.
- [57] Mašín D, Herle I. Improvement of a hypoplastic model to predict clay behaviour under undrained conditions. *Acta Geotechnica*. 2007;2(4):261-268.
- [58] Ragni R, Wang D, Mašín D, Bienen B, Cassidy MJ, Stanier SA. Numerical modelling of the effects of consolidation on jack-up spudcan penetration. *Computers and Geotechnics* 2016; 78:25-37.